Annual Report of 2007 Proposal (07103):

Proposal Title:	Seismic Characterization of Fault Damage and Healing over Multiple Length and Time Scales on the San Andreas Fault, Parkfield and the Calico Fault in the Eastern California Shear Zone
Proposal Category:	Data Gathering and Products Integration and Theory
Science Objectives:	A7, A8, A10, and D
Disciplinary Activities:	Seismology
Interdisciplinary Focus Area:	Fault Rupture Mechanics, Fault Damage and Healing over Multiple Length and Time Scales
Principal Investigators:	Yong-Gang Li at USC
Collaborative Investigators:	Elizabeth Cochran (UCSD)
Funding Agent:	Southern California Earthquake Center.
Amount of Award:	**$**20,000
Date:	February 1, 2007 to January 31, 2008.

During the period (02/01/2007 – 01/31/2008) of this proposal, we have completed the proposed work:

1. We shall use the existing FZTW data recorded the surface array in our previous experiments at Parkfield combined with the data recorded at borehole seismometers in the SAFOD main hole [*Malin et al.*, 2006] to obtain a more detailed LVZ damage structure along with the strike and depth of the SAF.

2. The InSAR data have shown strains at the Calico fault caused by the nearby Landers and Hector Mine earthquakes, indicating a compliant zone of reduced shear modulus on it. Under the NSF award, a group of scientists from UCSD, UCLA and USC deployed 100 seismometers in a square-shape array in 2006 to further investigate the width and depth extent of the compliance and damage on the CF [*Cochran et al.*, 2006b]. 3 shots were detonated within and off the fault zone. After explosions, the array works to record local, regional and teleseismic events for 6 months. The present proposal focuses on the 3-D modeling of FZTWs recorded generated by explosions and earthquakes located within the compliant zone. We shall resolve the fine internal structure within the compliant zone to further understand the stress localization in the fault zone.

I. San Andreas Fault damage at SAFOD viewed with fault-guided waves

Abstract Highly damaged rocks within the San Andreas fault zone at Parkfield form a low-velocity waveguide for seismic waves. Prominent fault-guided waves have been observed on the San Andreas Fault Observatory at Depth (SAFOD) seismographs, including a surface array placed across the fault-zone and a borehole unit placed in the SAFOD main hole at a depth of ~2.7 km below ground. The resulting observations are modeled here using 3-D finite-difference methods. To fit the amplitude, frequency, and travel-time characteristics of the data, the models require a downward tapering, 30-40-m wide fault-core embedded in a 100-200-m wide jacket. Compared with intact wall rocks, the core velocities are reduced by ~40% and jacket velocities by ~25%. Based on the depths of earthquakes generating guided-waves with long-duration wavetrains after the *S*-waves, we estimate that the low-velocity waveguide along the fault at the SAFOD site extends at least to depths of ~7 km. Thus it appears that significant damage zone exists at even twice the depths previously reported.

1. Introduction

Field and laboratory studies indicate that fault zones appear to undergo high, fluctuating, stresses and pervasive cracking during earthquakes [*Mooney and Ginzburg*, 1986; *Chester et al.*, 1993; *Andrews*, 2005]. However, due in part to their depth of burial, the magnitude and spatial extent of the resulting rock damages are not well constrained [*Hickman and Evans*, 1992; *Sleep et al.*, 2000]. The thickness and depth of such zones are critical ingredients in the understanding of fault mechanics [*Dieterich*; 1978; *Scholz*, 1990; *Rice*, 1992]. This article discusses these characteristics as recently observed with special fault-guided wave recordings at the San Andreas Fault Observatory at Depth (SAFOD) site near Parkfield, CA.

A zone of damaged rock surrounding the SAF at the SAFOD site has observed in previous studies using electromagnetic and seismic *P*- and *S*-wave travel time methods [*Unsworth et al*., 1997; *Thurber et al.*, 2003; *Roecker et al.*, 2004]. In these studies this zone is described as being a-little-as 200 hundred meters to as-much-as 1 km wide. The zone's observed seismic velocity reductions of 10-30% and *Vp/Vs* ratios approaching as-much-as 2.3 are thought to be caused by fracturing, brecciation, liquid-saturation, and high pore pressures. These features constitute a waveguide that traps seismic waves from earthquakes occurring within or close to it [*Li et al.*, 1990]. The amplitudes and dispersion feature of such trapped waves are known to be sensitive to the geometry and physical properties of the waveguide [*Li and Leary*, 1990; *Ben-Zion*, 1998]. At Parkfield, surface observations of fault-zone guided (trapped) waves suggest that a ~100-200-m zone of 20-40% *S*-wave velocity reduction exists to seismogenic depths [e.g. *Li et al.*, 1997, 2004a; *Malin et al.*, 1996; *Korneev et al.*, 2003]. Recently, SAFOD well logs from ~2.7 km underground have revealed a severely damaged zone around the San Andreas main fault characterized by highly fractured rock and multiple slip planes [*Hickman et al.*, 2005]. This ~200 m wide zone consists of a 30-40 m central core of ~40% lower seismic velocities surrounded by a ~25% lower velocity jacket inferred by fault guided PSV waves recorded at the seismograph installed in the SAFOD main hole at depth [*Ellsworth and Malin*, 2006].

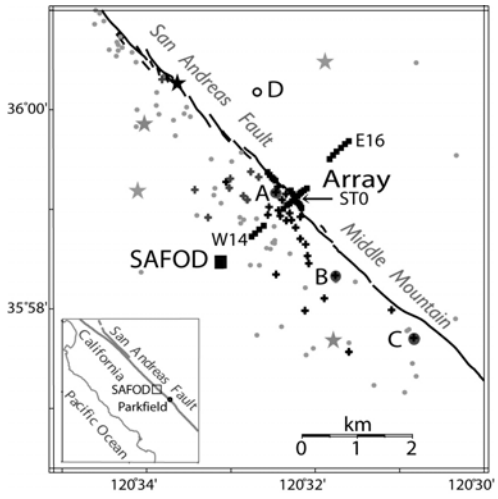

Figure 1 Locations of the study area (box in inset map), 45 portable seismographs (small squares) across and along the SAF near the SAFOD site (square), explosions (stars); and 120 microearthquakes (dots) recorded in the fall of 2003. Station ST0 of the array was located on the SAF surface trace; W14 and E16 on its west and east sides. Crosses denote 33 events generating fault-guided waves used in Fig. 4. Event A (solid circle), the SAFOD drilling target, occurred at ~2.7 km depth in 2003; its waveforms shown in Fig. 2c. Event B, a ~7 km deep aftershock of the 2004 *M*6 Parkfield earthquake, was recorded at the SAFOD main hole seismograph installed at ~2.7 km depth in 2005; its waveforms shown in Fig. 2d. Events C and D (solid and open circles) were deeper at 11 and 9 km, and were recorded on the surface array in 2003; their waveforms shown in Fig. 3.

2. Data and results

In fall 2003, as part of a site characterization program, an array of 45 portable seismographs was deployed across and along the surface trace of the SAF near SAFOD site [*Li et al.*, 2004b] (Fig. 1). About 120 local earthquakes were recorded at this surface array, including 33 events showing clear guide waves at depths between 2 and 12 km, from which the raypath incidence angles to ST0 are smaller than 30° from vertical. In December of 2004 and later a borehole seismograph was installed in the SAFOD mail hole at ~2.7 km depths where the SAF is characterized by a highly fractured and low velocity zone [*Ellsworth and Malin*, 2006] (Fig. 2a, b). Fig. 2c, d illustrate representative surface seismograms recorded at the surface array for a ~3 km-deep event (the SAFOD drilling target) in 2003 and borehole seismograms for a ~7 km-deep aftershock of the 2004 M6 Parkfield earthquake, showing the prominent fault guided waves which are simulated using the model in Fig. 2a.

Figure 3 shows 3-component seismograms recorded at the surface array in 2003 for 2 other representative earthquakes: events C and D of Fig. 1. The primary focuses here on these events are their relative relationships in terms of event location and recording points versus the types of waves generated and what these imply for the velocity structure of the SAF at SAFOD. There are two major points to be made in this regard, both illustrated more details in Fig. 4. The first point to be made is that the events whose locations and observation points appear closest to the projected trace of the SAF generate prominent fault guided waves characterized by relatively large amplitudes and long wavetrains following *S*-waves. The second point is that the time dispersion of the latter signals after *S*-waves is a strong function of event depth. Taken together, these two characteristics imply that the guided waves were traveling along a relatively continuous channel connecting the events and observation points.

These relations and the fault zone characteristics they imply were investigated further using a 3-D finite-difference waveform modeling code [*Graves*, 1996]. In this study, only the *S*-velocity related fault-zone trapped waves (FZTWs) were emphasized in the model computation. The study area was covered with a 10 m grid of computation point. A double-couple source is used for earthquakes while a point source used for explosions. The fault zone and surrounding rock velocity and attenuation in the model used for these simulations was built in several steps.

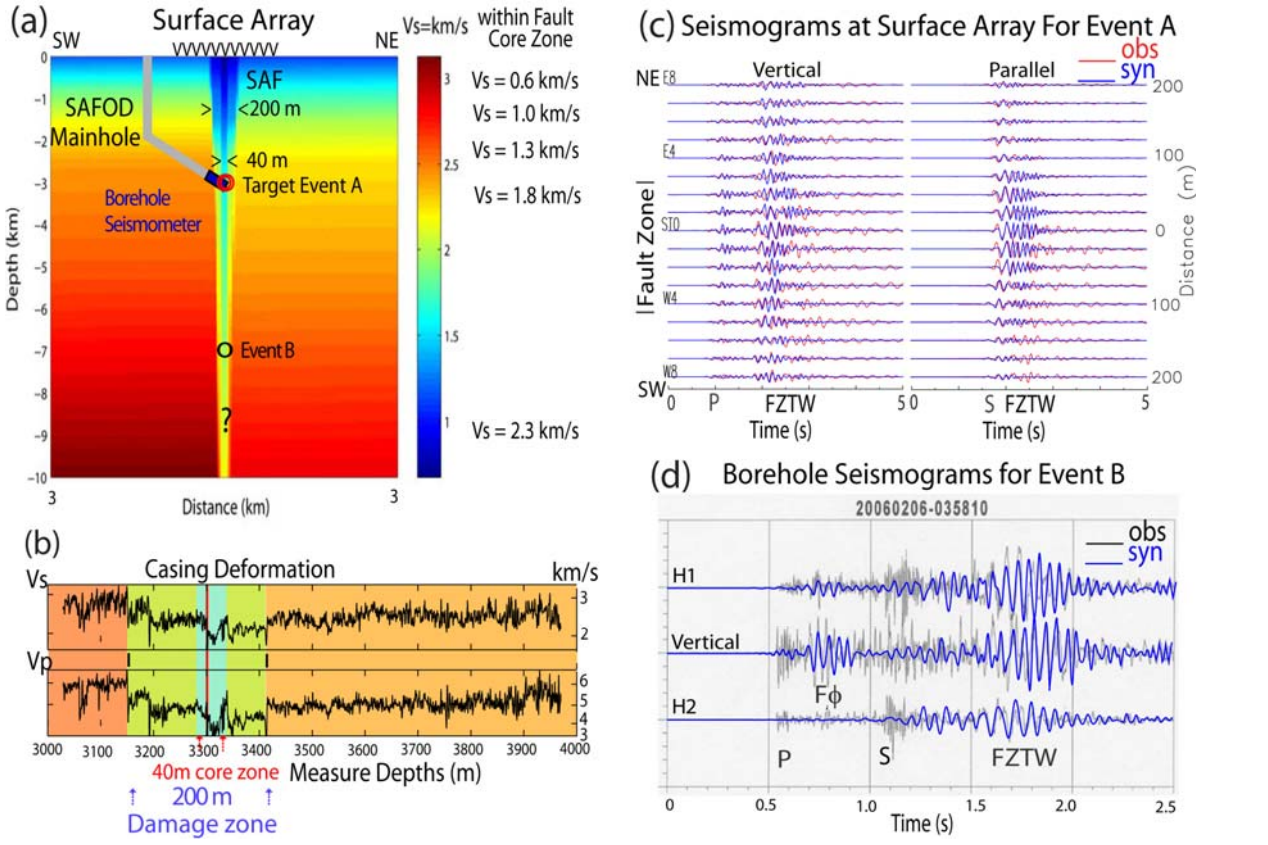

Figure 2 (a) Cross section near the SAFOD site showing the *S*-wave velocity model used in this study to compute synthetic fault-zone trapped waves (FZTWs) for the surface and borehole observations recorded in 2003 and 2005. Earthquakes A and B illustrate this type of fault guided waves used in this study. (b) Seismic velocities from SAFOD well logs showing the 40-m fault core and 200 m jacket low velocity damage zones. The red line indicates the location where fault creep is deforming the borehole casing. (c) Observed (red) and computed (blue) vertical- and parallel-component seismograms at the surface array for event A. The seismograms were low-pass filtered below 8 Hz and are plotted using a single global scale. (d) Observed and computed 3-component borehole seismograms recorded for event B. The synthetic seismograms have been low pass filtered below 12 Hz. The large signal between the P- and S- waves labeled $\mathbf{F_\phi}$ has been recently identified as a fault guided P-wave [*Malin et al.*, 2006; *Ellsworth and Malin*, 2006].

First, the direct and guided waves from explosions shown in Fig. 1 were modeled to obtain a velocity model for the upper 2 km of the SAFOD site and the shallow structure of the SAF as we did for modeling the FZTWs recorded in our previous experiment conducted near Parkfield [*Li et al.*, 2004a]. Then, using the well log velocities and 2005 borehole seismogram as calibration points, progressively deeper earthquakes with prominent guided waves were modeled by adjusting the fault structure immediately above their hypocenters. The velocities in surrounding rocks are constrained by tomography profiles obtained at Parkfield [*Thurber et al.*, 2003; *Roecker et al.*, 2004]. The result of this process is the downward tapered, two-layer, low-velocity fault zone sandwiched between different east and west sides of the SAF (Fig. 2a.). The waveform fits corresponding to this velocity model are shown in Fig. 2c, d. The synthetic seismograms fit amplitude behaviors and traveltimes of the FZTWs recorded at both the borehole seismograph and surface array stations within the fault zone as well as those east and west of the SAF. They also fit the depth dependant dispersion characteristics of both the on-fault and off-fault source-receiver relations seen in the data (Fig. 4c). We tested a shallow fault zone truncated at 4 km depth in modeling for the 11 on-fault events. Fig. 4d illustrates the synthetic seismograms showing nearly the same wavetrain length of FZTWs after the *S*-waves for events below 4 km and shorter than those seen in Fig. 4c.

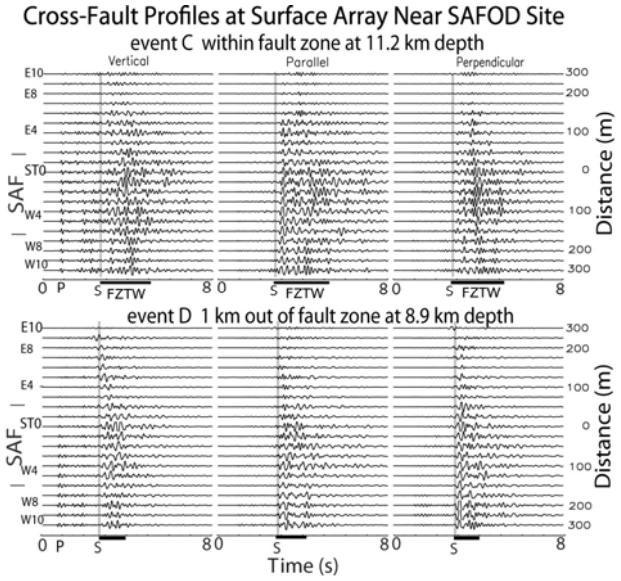

Figure 3 Three-component seismograms for events C and D. These representative seismograms were low-pass filtered below 6 Hz, aligned on the *S*-waves, and plotted with fixed amplitude scales for all traces in each plot. Fault-zone trapped waves (FZTW) with large amplitudes and long wavetrains after the S-arrivals are seen on the stations near the SAF surface trace at ST0 for the on-fault event C but not for the off-fault event D. Synthetic seismograms at station ST0 for these 2 events are shown in Fig. 4c.

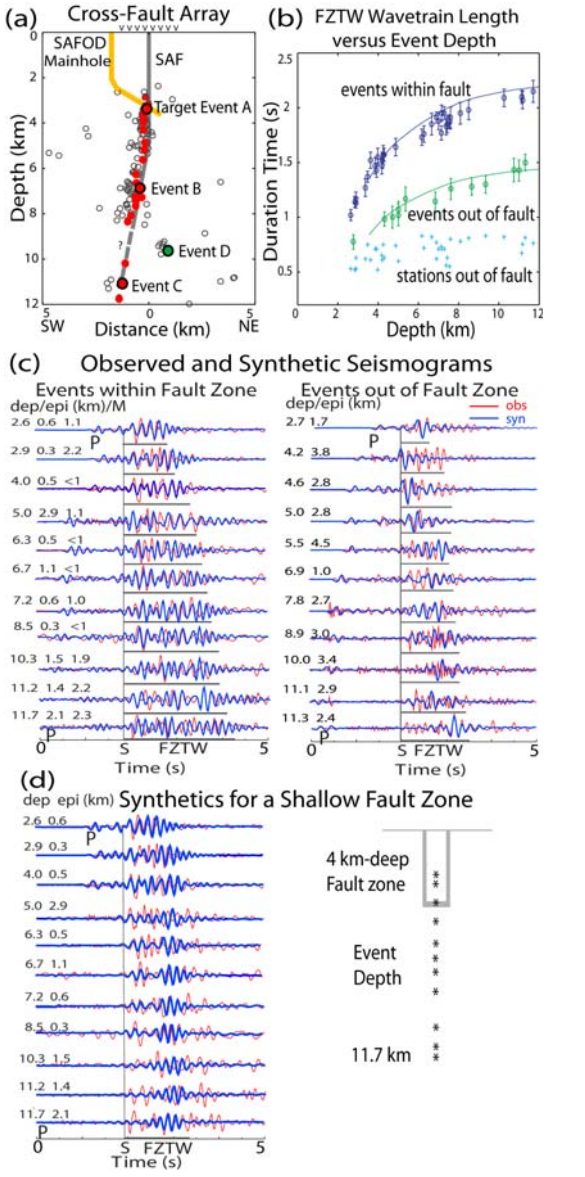

Figure 4 (a) Cross section through the SAF (grey line) at the SAFOD site showing locations of the microearthquakes (circles) with their epicenters shown in Fig. 1. Red circles mark 33 events showing strong fault-zone trapped waves (FZTW). Their epicenters are marked by crosses in Fig. 1. The locations of events A-D are also shown. (b) The measured time durations (denoted by blue circles) of FZTWs after *S* waves at stations within the fault zone for 33 on-fault earthquakes versus event depth, compared to those (green circles) measured at the same stations for off-fault earthquakes and those (blue crosses) at stations away from the fault zone for on- and off-fault events. Each data point is the average of 4 on- or off-fault stations. The error bars are standard deviations and the curves are polynomial fits to the data. (c) Observed and synthetic vertical-component seismograms at station ST0 for 11 on-fault and 11 off-fault earthquakes at different depths. *S*-arrivals for these events are aligned at the same time. The focal depth and epicentral distance from ST0 are plotted for each event. The finite-difference synthetic seismograms are computed using the model in Fig. 2a. Seismograms have been <8 Hz filtered and are plotted in trace-normalized. Bars denote the post-*S* wave durations, in which amplitude envelopes of FZTWs are above twice level in later coda. (d) Synthetic seismograms at ST0 for 11 on-fault events using a 4-km-deep fault zone.

Evidently, the SAFOD site guided waves can be explained in terms of a tapered, 30-40 m wide fault core of ~40% reduced velocity inside of a wider 100-200 m jacket of ~25% reduced velocity. The relatively intact rocks surrounding this composite damage zone have different velocities east and west of the SAF. Further, based on successful matching of the dispersion characteristics of the FZTWs following the *S*-waves as a function of depth, it would appear that, at least the low velocity jacket, and possibly its interior core, extends downward to no less than ~7 km (Fig. 4c). This is the depth inferred by the most clearly resolved and best fit guided waves seen in the SAFOD borehole seismograms [*Ellsworth and Malin*, 2006] that are modeled here (Fig. 2d).

3. Discussions and Conclusions

The damage zone at seismogenic depths may be caused by intense fracturing during earthquakes, including brecciation. Alternatively, given the fluid leakages currently taking place into the SAFOD well, the cause might relate to liquid-saturation and high pore-fluid pressure nears the fault. However, pore fluids arising from depth appear to hold a complex relationship with this damage zone, with its outer portions appearing to be more permeable than its core [Lockner et al., 2000]. Moreover, the damage zone may actually form more of a fluid barrier which fluids are simply pounded against. The damage zone is also asymmetric, apparently broader on the southwest side of the main fault trace. The asymmetry may imply that the fault has a moving damage zone or that when it ruptures it may preferentially damage the already weakened rocks [*Chester et al.*, 1993]. Alternately, greater damage may be inflicted in the extensional quadrant than the compressional quadrant near the propagating crack tip [*Andrews*, 2005]. Although the structural model shown in Fig. 2a accounts for the FZTWs and $\mathbf{F}_{\phi}$ observations and its parameters at ~3 km depth are confirmed by logging data, it is likely to represent a gross average of the actual fault-zone structure. The true structure in 3-D will certainly be more complicated, and the damage magnitude and extent will vary along the fault strike and depth due to rupture distributions and stress variations over multiple length and time scales.

References

Andrews, D. J. (2005), Rupture dynamics with energy loss outside the slip zone, *J. Geophys. Res., 110*, B01307, dio: 0.1029.

Ben-Zion, Y. (1998), Properties of seismic fault zone waves and their utility for imaging low-velocity structure, *J. Geophys. Res*., *103*, 12,567–12,585.

Chester F., Evans, J. and R. Biegel (1993), Internal structure and weakening mechanisms of the San Andreas fault, *J. Geophys. Res*., *98*, 771-786.

Dieterich, J. H. (1978), Time-dependent friction and the mechanics of strike-slip, *Pure Appl. Geophys*., *116*, 790-806.

Ellsworth, W. L., and P. E. Malin (2006), A first observation of fault guided PSV-waves at SAFOD and its implications for fault characteristics, *EOS, Transactions, and American Geophysics Union*, *87*, T23E-02, p154.

Graves, R. W. (1996), Simulating seismic wave propagation in 3D elastic media using staggered-grid finite differences, *Bull. Seism. Soc. Am*., *86*, 1091-1106.

Hickman, S. H., and B. Evans (1992), Growth of grain contacts in halite by solution-transfer: Implications for diagenesis, lithification, and strength recovery, in *Fault Mechanics and Transport Properties of Rocks*, pp. 253-280, Academic, San Diego, Cal.

Hickman, S. H., M. D. Zoback, and W. L. Ellsworth (2005), Structure and Composition of the San Andreas fault zone at Parkfield: Initial results from SAFOD Phase 1 and 2, *EOS, Transactions, and American Geophysics Union*, *83*, No.47, p237.

Korneev, V. A., R. M. Nadeau, and T. V. McEvilly (2003), Seismological studies at Parkfield IX: Fault-zone imaging using guided wave attenuation, *Bull. Seism. Soc. Am. 80*, 1245-1271.

Li, Y. G., P. Leary, K. Aki, and P. Malin (1990), Seismic trapped modes in Oroville and San Andreas fault zones, *Science*, *249*, 763-766.

Li, Y. G. and P. C. Leary (1990), Fault zone trapped seismic waves, *Bull. Seism. Soc. Am.*, 80, 1245-1271.

Li, Y. G., W. Ellsworth, C. Thurber, P. Malin, and K. Aki (1997), Observations of fault-zone trapped waves excited by explosions at the San Andreas fault California, *Bull. Seism. Soc. Am. 87*, 210-221.

Li, Y. G., J. E. Vidale, and E. S. Cochran (2004a), Low-velocity damaged structure on the San Andreas fault at Parkfield from fault-zone trapped waves, *Geophys. Res. Lett. 31*, L12S06, p1-5.

Li, Y. G., E. S. Cochran, and J. E. Vidale (2004b), Low-velocity damaged structure on the San Andreas Fault at seismogenic depths near the SAFOD drilling site, Parkfield, CA from fault-zone trapped waves, *EOS, Transactions, and American Geophysics Union*, *85*, No. 47, F1313.

Lockner, D., H. Naka, H. Tanaka, H. Ito, and R. Ikeda (2000), Permeability and strength of core samples from the Nojima fault of the 1995 Kobe earthquake, *USGS Open file, Report* 00-129, 147-152.

Malin, P. E. M. Lou, and J. A. Rial (1996), $\mathbf{F_R}$ waves: A second fault-guided mode with implications for fault property studies, *Geophysical Research Letters*, *23*, 3547 – 3550.

Malin, P. M., E. Shalev, H. Balven, and C. Lewis-Kenedi (2006), Structure of the San Andreas Fault at SAFOD from P-wave tomography and fault-guided wave mapping,, *Geophys. Res. Letter 33*, No. 13, pp. 13314, 2006GL025973.

Mooney, W. D. and A. Ginzburg (1986), Seismic measurements of the internal properties of fault zones, *Pure Appl. Geophys. 124*, 141-157.

Rice, J. R. (1992), Fault stress states, pore pressure distributions, and the weakness of the San Andreas fault, in *Fault Mechanics and Transport Properties of Rocks*, edited by B. Evans and T.-F. Wong, 475-503, Academic, San Diego, Calif.

Roecker, S., C. Thurber, and D. McPhee (2004), Joint inversion of gravity and arrival times data from Parkfield: New constraints on structure and hypocenter locations near the SAFOD drill site, *Geophys. Res. Lett., 31*, DOI 10.1029/2003GL019396.

Scholz, C. H. (1990), *The Mechanics of Earthquakes and Faulting*, Cambridge Univ. Press, New York.

Sleep, N. H., E., Richardson, and C. Marone (2000) Physics of friction and strain rate localization in synthetic fault gouge, *J. Geophys. Res. 105*, 25,875-25,890.

Thurber, C., S. Roecker, K. Roberts, M., Gold, L. Powell, and K., Rittger (2003), Earthquake location and 3-D fault zone structure along the creeping section of the San Andreas fault near Parkfield, CA: Preparing for SAFOD, *Geophys. Res. Lett*. ***30***, 1112-1115.

Unsworth, M., P. Malin, G. Egbert, and J. Booker (1997), Internal structure of San Andreas fault at Parkfield, CA, *Geology*, 356-362.

We have examined more data recorded at the borehole seismographs installed in the SAFOD mainhole at ~3 km depth where the San Andreas fault zone passing, and in the pilot hole drilled 1.8 km away fault the SAF. Prominent fault-zone trapped waves generated by Parkfield aftershocks occurring at different depths and epicentral distances within the fault zone arrive at the mainhole seismograph but not at the pilot-hole seismograph, indicating the low-velocity damage zone (waveguide) on the SAF extending along the fault strike across the seismogenic depths.

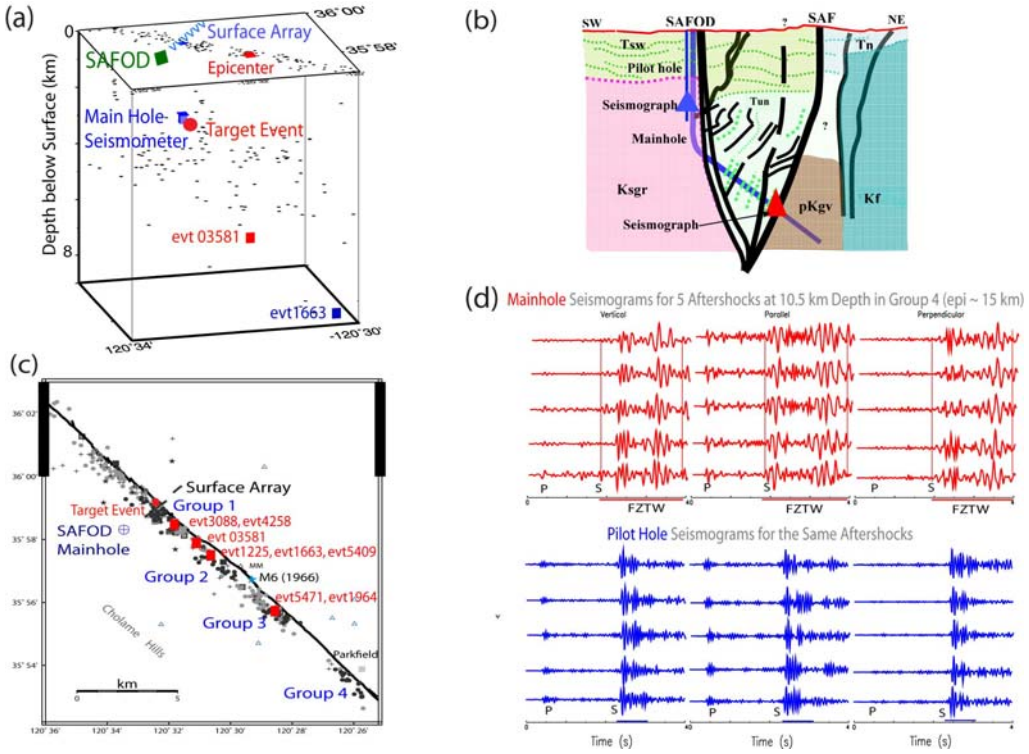

Figure 5. (a) 3-D view of locations of aftershocks (black dots) of the 2004 M6 Parkfield earthquake recorded at the SAFOD Main Hole seismograph (blue box) that was installed at the depth of ~3 km. (b) SW-NE cross section along the Phase 2 SAFOD Main Hole toward the surface trace of the SAF. The borehole seismographs installed in the SAFOD mainhole and pilot hole (denoted by red and blue triangles). The geological interpretation is based on the results of a Drill Bit Seismic reflection profile gathered during the 2004 Phase 1 drilling [Ellsworth and Malin, 2006]. (c) Map view shows aftershocks recorded at SAFOD borehole seismographs in 2004 and 2005. (d) 3-component seismograms recorded at SAFOD mainhole and pilot hole seismographs for 5 on-fault aftershocks of the 2004 M6 Parkfield earthquake show prominent fault-zone trapped waves (FZTW) with large amplitudes and long wavetrains after S-waves at the mainhole seismograph located within the fault zone but not at the pilot-hole seismograph 1.8 km away from the fault, indicating a low-velocity waveguide (damage zone) existing along the SAF strike and with depth.

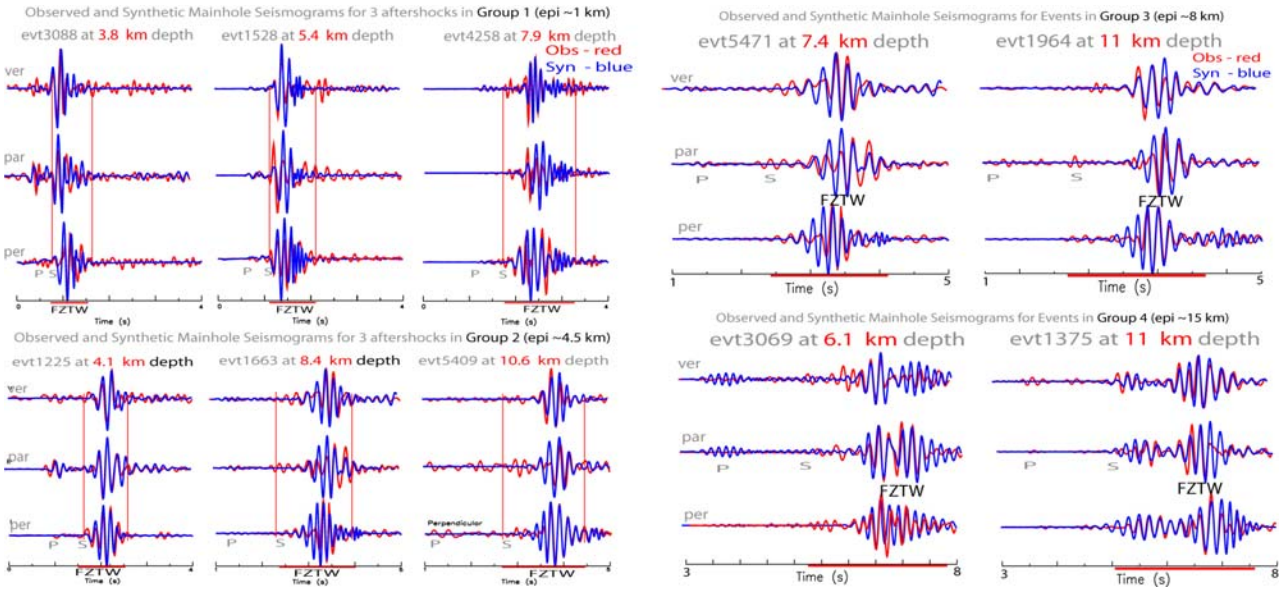

Figure 6. (a) Observed and 3-D finite-difference seismograms at SAFOD mainhole seismograph for Parkfield aftershocks occurring within the fault zone at different depths and epicentral distances show prominent fault-zone guided waves, the wavetrain length of which increases as the travel distance increases along the fault strike or with the depth, suggesting a continuous low-velocity damage zone on the SAF extending across seismogenic depths. The model in Fig. 2a is used in waveform computation.

II. Understanding fault zone compliance: Seismic probing of InSar anomalies

The InSAR data have shown anomalous strains at the Calico fault caused by the nearby Landers and Hector Mine earthquakes, indicating a compliant zone of reduced shear modulus on it [*Fialko*, 2002, 2004]. We deployed 100 seismometers of a square-shape array at the CF in Mojave Desert in 2006 to further investigate the fault-zone compliance (Fig. 7a). 3 shots were detonated within and off the fault zone. After explosions, the array works to record earthquakes for 6 months. Fig. 7b&7c exhibit seismograms recorded at cross-fault line B for shot SP1 and a quarry blast located within and close to the fault zone, showing fault-zone trapped waves at stations within a ~1,2 km-wide zone around the CF.

We have obtained the preliminary results from tomography and fault-zone trapped wave modeling for the data for explosions and local earthquakes show a 1 to 2 km wide low-velocity zone (LVZ) on the Calico fault extending to the depth of at least 5-7 km, in good agreement with the InSAR-derived compliant zone [*Fialko et al.*, 2002; *Fialko*, 2004]. The initial analysis of the data that indicate along-strike variations in the degree of damage, with a wider, or perhaps more severe damage zone on the Calico fault to the northwest of the array than to the southeast [Cochran et al., 2006, 2007; Li 2007]. For example, we used velocity models in Fig. 7d to compute 3-D FD synthetic FZTWs best fitting observations (Fig. 7e). We further examined the data from a quarry blast and 4 micro-earthquakes located within the compliant zone of the Calico fault. The profiles Fig. 8 show prominent fault-zone trapped waves at stations within the low-velocity zone along the Calico fault. Observations and 3-D finite simulation of fault zone trapped waves for these events allow us to obtain a structural model across the Calico fault as shown in Fig. 9. The model inferred by FZTWs generated by shots and quarry blast are consistent with the result from tomography using first *P*-arrival times. The low-velocity compliant zone likely extends to the depth of at least below 5 km. In the next step, we shall use the data recorded at our seismic array for telemetric earthquakes to document the deep portion of the compliant zone on the Calico fault. We also find that FZTWs are most prominent in the fault core within the compliant damage zone, which might be related to the latest major earthquake on the CF.

These findings indicate that faults can affect rock properties at significant distances from the primary fault slip surfaces, a result with implications for the portion of energy expended during rupture to drive the cracking and yielding of rock. The data from more local earthquakes and telemetry events are in processing and modeling. We expect that these data allow us to obtain a detailed depth extension of the LVZ damage on the Calico fault. We thus aim to reconcile the seismic and InSAR anomalies to produce an integrated structural model of the damage zone around a major strike-slip fault. The preliminary results from this project have been reported in a special session at Fall AGU meeting, the EarthScope National Annual Meeting and SSA Annual Meeting in 2007.

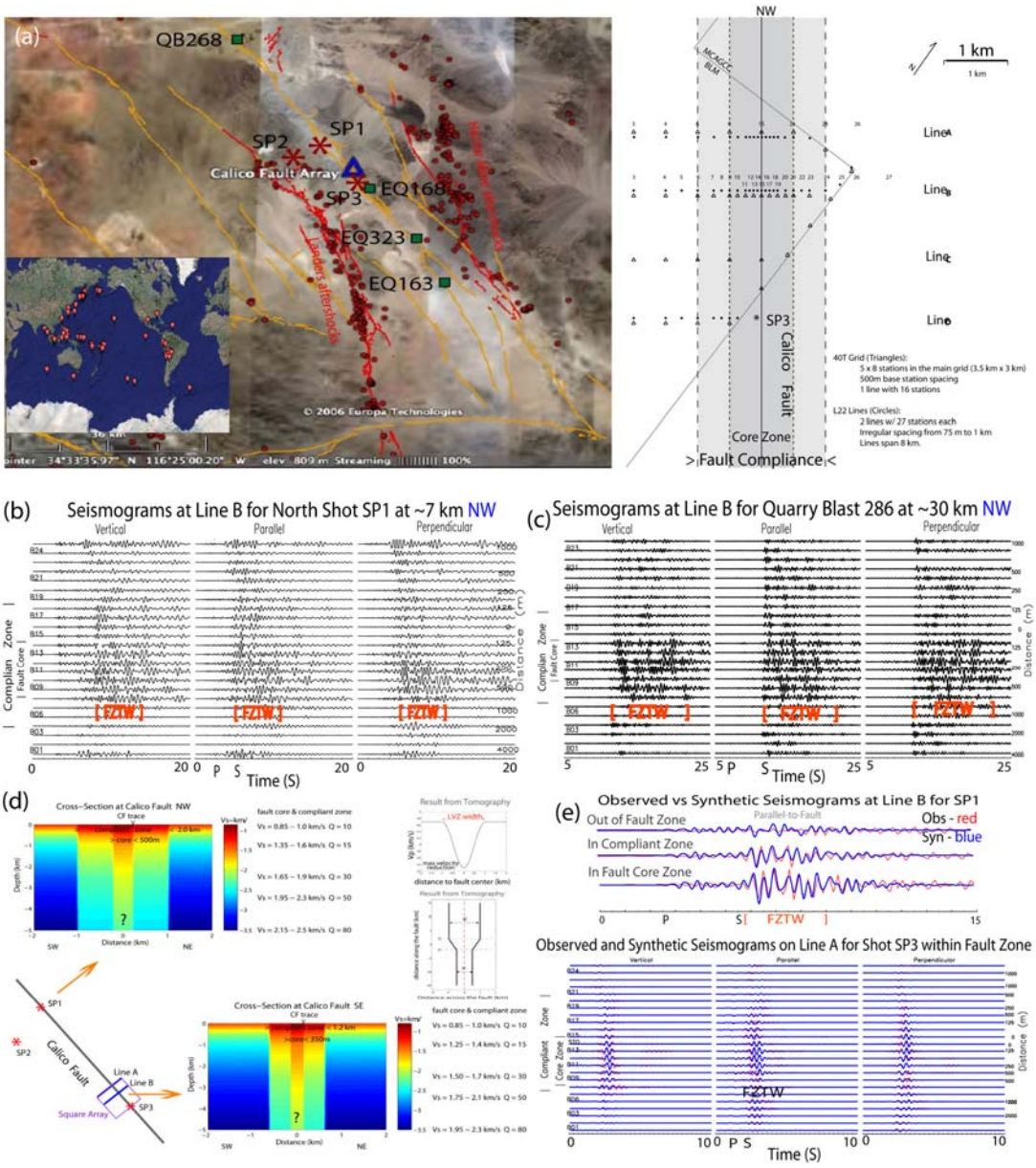

Figure 7 (a) Left: Map shows locations of hundreds of local earthquakes (red circles) recorded at our seismic array (blue triangle) deployed at the Calico fault (CF) in Mojave Desert in 2006. Many of them are aftershocks of the M7.4 Landers and M7.1 Hector Mine earthquakes. Inset: Telemetry earthquakes with the Largest event: M7.7 on July 17, 2006 in Indonesia, recorded at our seismic array at the CF. Right: The layout of seismic array. (b) Three-component seismograms recorded at the cross-fault Line B for explosion SP1 detonated within the fault zone show fault zone trapped waves (FTZW) at stations within a ~1-2-km-wide low velocity compliant zone, and most prominent in the ~350-m-wide fault core zone. (c) Seismograms recorded at Line B for a quarry blast QB268, ~30 km NW of the seismic array, show FZTWs with longer wavetrains than those from SP1 although the wavetrain length of FZTWs is not linearly proportional to the distance because FZTWs from quarry blaster travel in the deeper portion of the fault zone. (d) Left: The cross-fault sections of the structural models at shallow depth for the Calico fault at shot-hole site of SP1 and the seismic array site, respectively. The models are used to the best fit of synthetic waveforms and arrival times to observed seismograms. The velocities and Q values are depth-dependent. The widths of the compliant zone and fault damaged core zone vary along the fault strike, wider as the zone approaches to the northwest edge of the working area between SP1 and SP3. The waves from explosion and quarry blast can penetrate at the shallow at 2-3 km. The depth range in these models is uncertain. It will be determined in the next step of simulations for FZTWs from earthquakes. Right: The P-wave velocity profiles across and along the Calico fault obtained from tomography using first P-arrivals of 3 explosions and local earthquakes, in generally consistent with the structural models obtained from simulations of FZTWs. (e) Top: Observed and FD synthetic seismogram at 3 stations of Line B located on close and away from the CF. Seismograms are <5 Hz filtered. Bottom: Observed and FD synthetic seismograms at cross-fault line A for shot SP3. The synthetic seismograms are computed using the model in Fig. 7d. A point source is located in the fault core zone at distance 3 km from Line A, and at 7.5 km from Line B, respectively. Synthetic seismograms have been <3 Hz filtered.

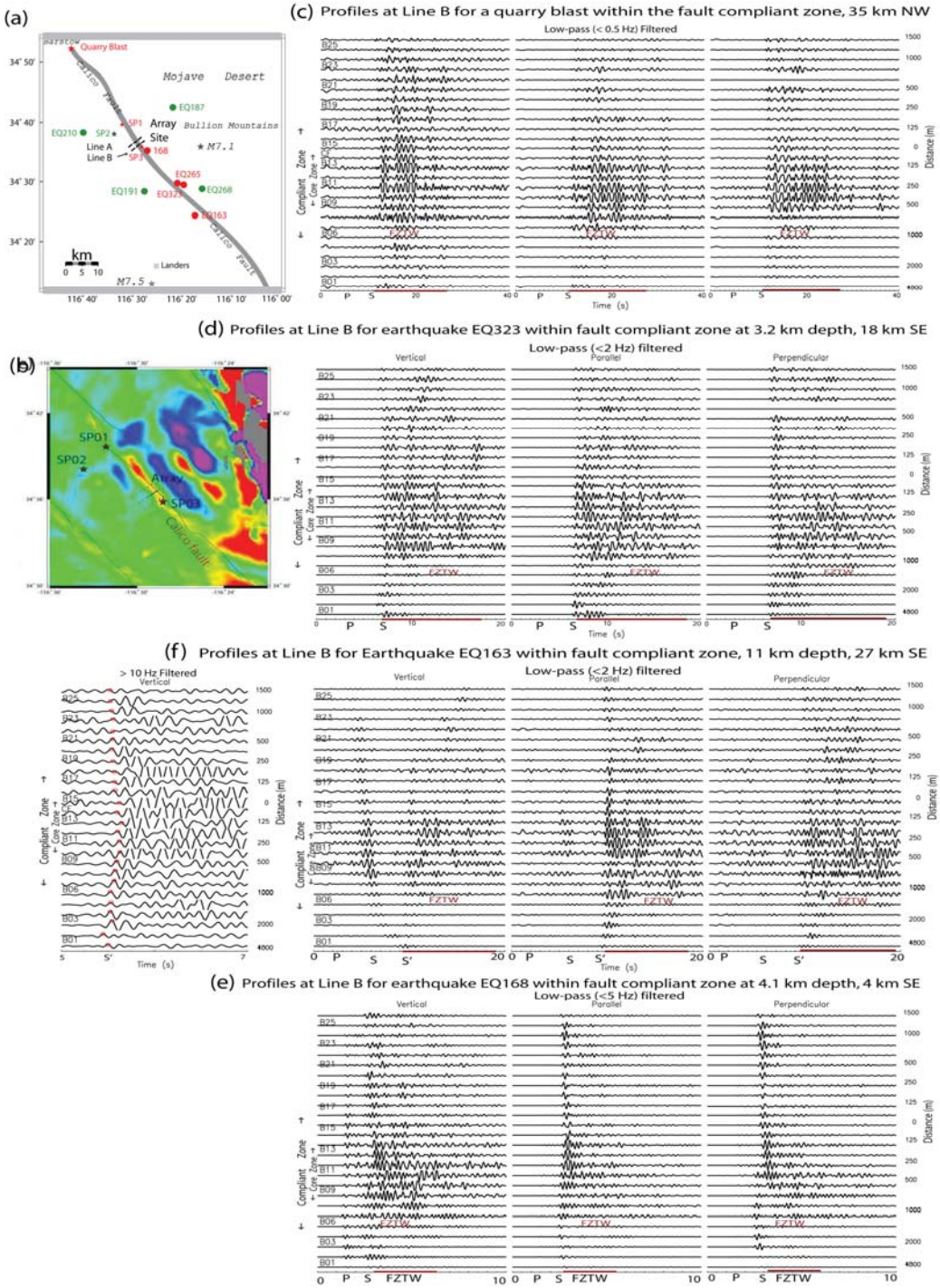

Figure 8 (a) Left: Map shows locations of a quarry blast and 8 earthquakes occurring within (red circles) and out of (green circles) local earthquakes recorded at Line A and Line B (dashed lines) of our seismic array across the Calico fault (CF) in Mojave Desert in 2006. The waveform data from these events have been simulated using 3-D finite difference code in terms of the structural model shown in Fig. 7d and Fig. 9. (b) InSar data show strain anomalies caused by dynamic stress changes due to the 1999 M7.1 Hector Mine earthquake, with obvious ascending slip along the Calico fault due to its low-rigidity compliance. Note that the 1-2-km-wide compliant zone along the Calico fault strike is broader toward NW of the seismic array. (c), (d) and (e) Three-component seismograms recorded at Line B across the Calico fault for a quarry blast, a shallow earthquake and a deep earthquake located within the fault compliant zone generating prominent fault zone trapped waves (FZTW). Red bars show the time duration of FZTWs after S-waves. Note that the time duration of FZTWs increases as travel distance increases along the fault strike and with depth, suggesting that the LVZ zone on the Calico fault likely extends across seismogenic depths although the compliance is weaker with depth. The first P-arrivals in the time-expanded plot for the deep event show time delays at stations located within the 1-1.5-km-wide low-velocity fault damage zone.

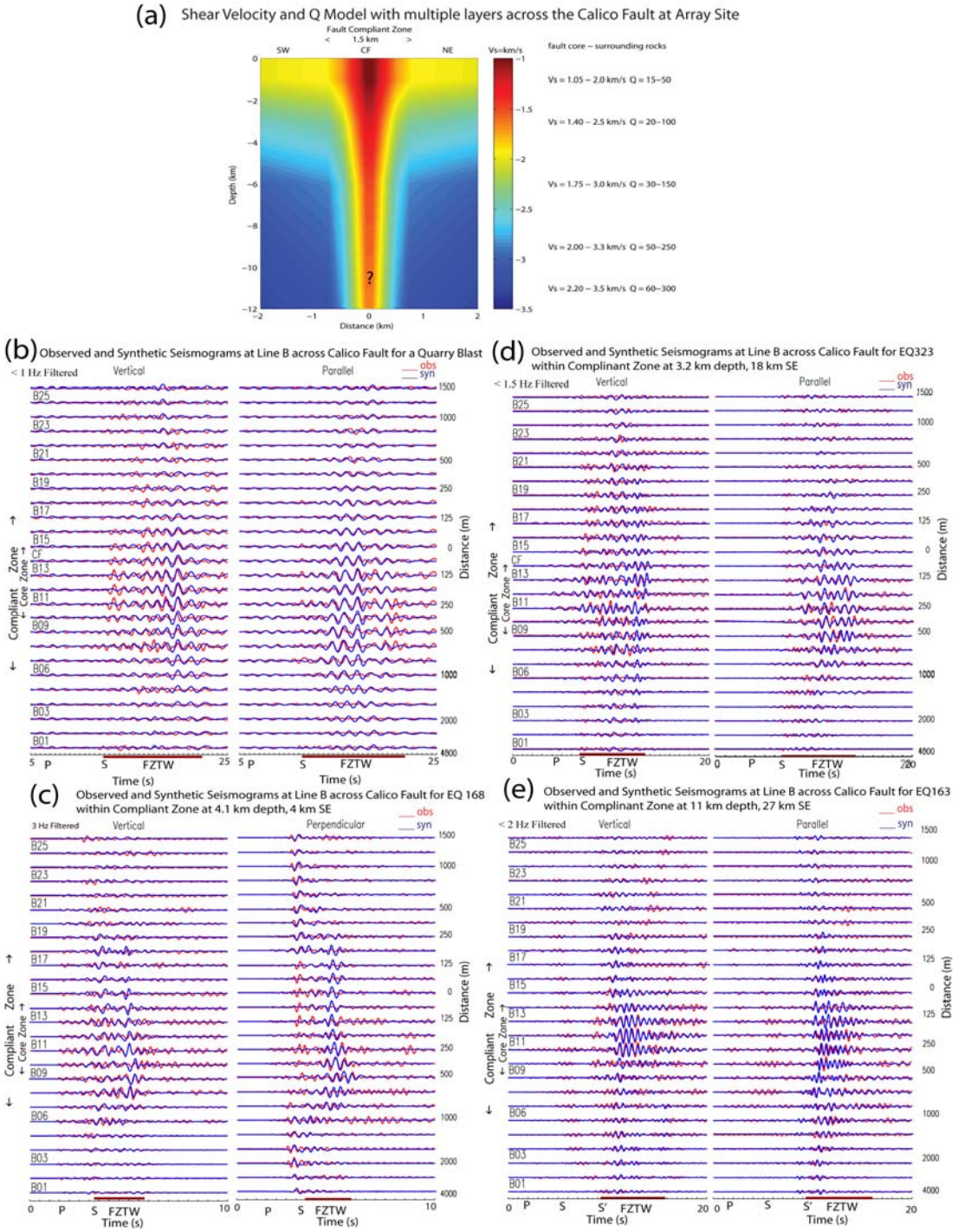

Figure 9 (a) The vertical section across the Calico fault shows the model at the array site including a 1.5-km-wide low-velocity compliant zone with velocity reduction of 10-45% from wall rocks to the center of the fault zone. The velocities and *Q* values in the model are also depth dependent, with greater velocity reduction and smaller *Q* at shallower depth. The width of the fault compliant zone is 2-km wide toward NW. This model is updated from the original model (Fig. 7d) from first-round computation of FZTWs generated by near-surface explosions. In the updated model, the LVZ compliant zone extends to the deep level although with less velocity reduction than those at the shallow depth because the confined pressure increases with depth. The velocity changes laterally across the fault strike with a gentle gradient within the 1-1.5-km-wide fault compliant zone, consistent with that obtained from 3-D P-arrival tomography (see Fig. 7d). (b)-(e) Observed and 3-D finite-difference synthetic seismograms at cross-fault Line B for a quarry blast located 35-km NW and earthquakes EQ168, EQ323 EQ163 located at different depths and distances from the array site (see Fig. 8a). All these events are located within the fault compliant zone. Synthetic seismograms are computed using the velocity model shown in Fig. 9a. An explosion point source used for quarry blast while a double-couple source used for earthquakes in computation.

Yong-Gang Li's Bibliographic Reference During the Period of 2006-2007

(December 20, 2007)

Li, Y. G., and P. E. Malin, San Andreas Fault damage at SAFOD viewed with fault-guided waves, *Geophys. Res. Lett.*, in review, 2007. SCEC Contribution Number **1128**.

Li, Y. G., P. E. Malin and J. E. Vidale, Parkfield fault-zone guided waves: Low-velocity damage zone on the San Andreas fault at depth near SAFOD site at Parkfield by fault-zone trapped waves, *Scientific Drilling*, Special Issue, No. 1, doi:10.2204 /iodp.sd.s01.09, 73-77, 2007. SCEC Contribution Number **1139**.

Li, Y. G., P. Chen, E. S. Cochran, and J. E. Vidale, Seismic velocity variations on the San Andreas Fault caused by the 2004 *M*6 Parkfield earthquake and their implications, Earth, Planets and Space, 59, 21-31, 2007. SCEC Contribution Number **962**.

Li, Y-G, P. Chen, E. S. Cochran, J. E. Vidale, and T. Burdette, Seismic Evidence for Rock Damage and Healing on the San Andreas Fault Associated with the 2004 M6 Parkfield Earthquake, The Bulletin of Seismological Society of America, Andy Michael, Seismological Society of America, El Cerrito, V96, Parkfield Special Issue, S349-S363, 2006. SCEC Contribution Number **924**.

Cochran, E. S., Y.-G. Li and J. E. Vidale, Anisotropy in the Shallow Crust Observed around the San Andreas Fault Before and After the 2004 M 6.0 Parkfield Earthquake, Bulletin of the Seismological Society of America, V96, Parkfield Special Issue, S364–S375, 2006. SCEC Contribution Number **1080**.

Conference Abstracts:

Li, Y.-G., P. E. Malin, J. E. Vidale, and E. S. Cochran, High-resolution imaging of the San Andreas Fault from fault-zone trapped waves recorded at the SAFOD borehole seismograph and surface array, *EOS*, T53C-04, pp168, Fall AGU Meeting, 2007.

Malin, P. E., Y.-G. Li, P. Chen, E. S. Cochran, and J. E. Vidale, Seismic Documentation for Rock Damage and Heal on the San Andreas Fault Involved in the 2004 *M*6 Parkfield Earthquake, *EOS*, S43A-1048, pp74, Fall AGU Meeting, 2007.

Cochran, E. S., Y.-G. Li, P. M. Shearer, J. E. Vidale, and Y. Fialko, Calico fault structure determined using traveltime data from seismicity and explosions, *EOS*, T54A-01, pp178, Fall AGU Meeting, 2007.

Li, Y.-G., and P.E. Malin, Space/time property variations on the Parkfield San Andreas from fault guided waves, EarthScope National Annual Meeting, Monterey CA, March, 2007.

Li, Y.-G., J. E. Vidale, E. S. Cochran, and P. Chen, Rock damage and heal on the San Andreas Fault involved in the 2004 *M*6 Parkfield earthquake, EarthScope National Annual Meeting, Monterey, CA, March, 2007.

Cochran, E. S., Y. G. Li, P. M. Shearer, J. E. Vidale, and Y. Fialko, The Calico fault zone: Preliminary seismic evidence for a wide damage zone, EarthScope National Annual Meeting, Monterey CA, March, 2007.

Cochran, E. S., Y. G. Li, P. M. Shearer, J. E. Vidale, and Y. Fialko, Seismic evidence for a wide damage zone around the Calico Fault, Seism. Soc. Am. Annual Meeting, April, 2007.